Investigations of cardiac fibrosis rheology by *in vitro* cardiac tissue modeling with 3D cellular spheroids

Michele Zanetti [a,b,*,3,1], Nicoletta Braidotti [a,b,**,3,2], Maydha Khumar [c], Efren Montelongo [c], Raffaella Lombardi [d,e], Orfeo Sbaizero [d,f], Luisa Mestroni [d,e], Matthew R.G. Taylor [d], Gabriele Baj [g], Marco Lazzarino [a], Brisa Peña [c,d,e], Laura Andolfi [a]

[a] *Consiglio Nazionale Delle Ricerche-Istituto Officina Dei Materiali (CNR-IOM), Area Science Park Basovizza, Strada Statale 14, Km 163,5, 34149, Trieste, Italy*
[b] *Department of Physics, University of Trieste, Via A. Valerio 2, 34127, Trieste, Italy*
[c] *Bioengineering Department, University of Colorado Denver Anschutz Medical Campus, At Bioscience 2 1270 E. Montview Avenue, Suite 100, Aurora, CO, 80045, United States*
[d] *Department of Medicine, Division of Cardiology, University of Colorado Anschutz Medical Campus, At 12700 E.19th Avenue, Bldg. P15, Aurora, CO, 80045, United States*
[e] *Cardiovascular Institute, University of Colorado Denver Anschutz Medical Campus, School of Medicine, Division of Cardiology, At 12700 E.19th Avenue, Bldg. P15, Aurora, CO, 80045, United States*
[f] *Department of Engineering and Architecture, University of Trieste, Via A. Valerio 6/A, 34127, Trieste, Italy*
[g] *Department of Life Sciences, University of Trieste, Via L. Giorgieri 5, 34127, Trieste, Italy*

ARTICLE INFO

Keywords:
Cardiac fibrosis
Cardiac spheroids
Stress relaxation
Rheological behavior
3D cellular model
AFM

ABSTRACT

Cardiac fibrosis refers to the abnormal accumulation of extracellular matrix within the cardiac muscle, leading to increased stiffness and impaired heart function. From a rheological standpoint, knowledge about myocardial behavior is still lacking, partially due to a lack of appropriate techniques to investigate the rheology of *in vitro* cardiac tissue models. 3D multicellular cardiac spheroids are powerful and versatile platforms for modeling healthy and fibrotic cardiac tissue *in vitro* and studying how their mechanical properties are modulated. In this study, cardiac spheroids were created by co-culturing neonatal rat ventricular cardiomyocytes and fibroblasts in definite ratios using the hanging-drop method. The rheological characterization of such models was performed by Atomic Force Microscopy-based stress-relaxation measurements on the whole spheroid. After strain application, a viscoelastic bi-exponential relaxation was observed, characterized by a fast relaxation time (τ_1) followed by a slower one (τ_2). In particular, spheroids with higher fibroblasts density showed reduction for both relaxation times comparing to control, with a more pronounced decrement of τ_1 with respect to τ_2. Such response was found compatible with the increased production of extracellular matrix within these spheroids, which recapitulates the main feature of the fibrosis pathophysiology. These results demonstrate how the rheological characteristics of cardiac tissue vary as a function of cellular composition and extracellular matrix, confirming the suitability of such system as an *in vitro* preclinical model of cardiac fibrosis.

1. Introduction

Myocardial fibrosis (MF) refers to the pathological deposition of a fibrotic scar within the myocardium. Such condition poses significant threats to heart function and is associated with several cardiac diseases (Diamond et al., 2005; Schultheiss et al., 2019; Gheorghiade et al., 2006). MF is marked by an altered cellular composition, characterized by cardiomyocytes loss followed by fibroblast activation and proliferation, culminating into myofibroblasts-driven accumulation of extracellular matrix (ECM) (Davidson et al., 2020; Frangogiannis, 2021;

* Corresponding author. Department of Physics, University of Trieste, Via A. Valerio 2, 34127, Trieste, Italy.
** Corresponding author. Department of Physics, University of Trieste, Via A. Valerio 2, 34127, Trieste, Italy.
E-mail addresses: michele.zanetti@yale.edu (M. Zanetti), nbraidotti@units.it (N. Braidotti).
[1] Present address: Department of Biomedical Engineering, Yale University, 17 Hillhouse Ave, New Haven, Connecticut, 06511, United States.
[2] Present address: Department of Chemical and Pharmaceutical Sciences, University of Trieste, Via L. Giorgieri 1, 34,127, Trieste, Italy.
[3] These authors contributed equally to the manuscript.

Vukicevic et al., 2022). The resulting fibrosis induces electrical disturbances and myocardial stiffening which in turn reduce the heart compliance, affecting its ability to contract and relax, ultimately leading to ventricular dysfunction (Davidson et al., 2020; Aghajanian et al., 2019; Travers et al., 2016). It is well known that ventricular function is greatly influenced by the myocardium's mechanical properties (Emig et al., 2021; Guo et al., 2021), and a growing amount of research pointed out the existence of hysteresis in its stress-strain relationship (Demer et al., 1983; Liu et al., 2022), calling for a broad investigation of its passive viscoelastic behavior. Indeed, the ventricular free wall displays an anisotropic viscoelastic behavior, meaning that its mechanical properties change along different directions, presenting both elastic and viscous properties while being deformed (Liu et al., 2022). Such viscoelasticity has been investigated at different scales, using distinct techniques. Tensile and stress-relaxation tests, for example, were performed onto centimeter and millimeter-sized fresh explants, showing nonlinear viscoelastic properties (Hassan et al., 2012).

The knowledge of the heart mechanical signature lays the foundations for a more accurate investigation of the MF pathology. Indeed, *in vitro* disease modeling allows to study MF effects on the heart tissue on a functional level, thus helping to develop new treatments for it.

Recently, Cardiac Spheroids (CSs) were introduced as simple *in vitro* three-dimensional (3D) models to study the heart microenvironment (Polonchuk et al., 2017). Their cell population can be tuned by including different ratios of multiple cell types, such as cardiomyocytes, fibroblasts, and endothelial cells, potentially mimicking the same ratios as the *in-vivo* heart tissue. In a similar study (Figtree et al., 2017), hanging drop mixed 3D cultures of neonatal rat ventricular myocytes (NRVMs), and their non-myocyte counterparts, were created. The resulting CSs were then treated with transforming growth factor beta 1 (TGFβ1), a known profibrotic agent (Leask, 2007), causing a dramatic increase in collagen deposition as well as elevated expression levels of fibronectin and connective tissue growth factor.

Although these basic 3D models have already shown their efficacy in reproducing the intricate microenvironment of MF (Polonchuk et al., 2017; Figtree et al., 2017), the assessment of their viscoelastic properties represents a significant technological challenge, mainly because of their size (from 100 μm, up to a millimeter in diameter). At larger scales, the rheological properties of tissue biopsies and ex-vivo tissue explants are effectively characterized by macro-scale techniques (Cheng et al., 2008; Parkins et al., 2021). On the other hand, viscoelasticity at the single-cell level and sub-cellular structures (e.g. nuclei and lamellipodia), is better studied using micro- and nanoscale methods such as atomic force microscopy (AFM) (Chim et al., 2018; Rother et al., 2014; Mahaffy et al., 2004; Andolfi et al., 2023). To bridge this gap while leveraging the great sensitivity and versatility of the AFM, we have already shown how to perform stress-relaxation measurements on CSs by parallel plate rheology using custom-fabricated macro-cantilevers (Zanetti et al., 2022; Andolfi et al., 2019).

Here, the viscoelasticity of co-cultured CSs with a growing fibroblast proportion was characterized by the same approach. We used three different ratios of cardiac myocytes and fibroblasts to mimic a healthy condition, as compared to two fibrotic ones, investigating how an increased fibroblast density affects the mechanical characteristics of CSs. We demonstrated that, as the ratio of fibroblasts increases, the rheological properties of CSs change, accompanied by an increase of collagen levels. Besides, these findings suggest that such approach can be considered a valuable tool to investigate in *vitro* effects of antifibrotic therapies and their ability to restore a physiologically native mechanical environment.

2. Materials and methods

2.1. Cardiomyocytes and cardiac fibroblasts isolation procedure

Neonatal Rat Ventricular Cardiomyocytes (NRVMs) and Neonatal Rat Ventricular Fibroblasts (NRVFs) were extracted from P4-5 Wistar rat hearts as previously described (the study was conducted according to the guidelines of the Declaration of Helsinki and approved by the OPBA Committee of the University of Trieste, under the Italian Ministry of Education, University, and Research, Protocol Code 1FF80.N.PZB) (Zanetti et al., 2022; Braidotti et al., 2022). Briefly, animals were euthanized by decapitation, and their hearts excised and minced down to ~1 mm fragments. The tissue was then digested by trypsinization over 3 h under continuous agitation, while the supernatant was being neutralized in calf serum (Sigma® 12133C) and exchanged with fresh trypsin buffer every 5 min. Endothelial cells were discarded over the first two steps of such trypsinization process. Cells mixture (NRVMs and NRVFs) were sedimented at 300 RCF for 10 min and resuspended in fresh media (MEM supplemented with 5% calf serum, 1% penicillin-streptomycin, 10 mg/L vitamin B12) at a density of 5×10^5 cells/mL.

2.2. Separation of NRVMs from NRVFs in 2D culture

The cells mixture resulting from the isolation procedure was strained through a 40 μm (pore size) filter and pre-plated in two separate 96 mm ø tissue culture dishes. After 45 min of pre-plating, >90% of NRVFs adhered to the dish surface, while the floating portion contained mainly NRVMs with residual NRVFs. Then, NRVMs in the floating portion were collected and re-plated in a separate, gelatin-coated dish, at 1×10^5 cells/cm^2, while fresh media was fed to the NRVFs attached portion.

2.3. Cardiac spheroids assembly

After being cultured for four-days in 2D plates, NRVMs and NRVFs were harvested. NRVMs and NRVFs monolayers were washed with phosphate buffer saline (PBS) and detached by trypsinization over 5 min. Trypsin was neutralized with fresh media, cells were counted, and NRVMs/NRVFs were collected in two separate 15 mL tubes and sedimented at 100 RCF for 5 min. Each pellet was resuspended separately, at 2.5×10^6 cells/mL in fresh media. For clarity, we will refer to these high-density cell suspensions as "stock NRVMs" and "stock NRVFs".

It is important to mention that, as specified above, the cell pre-plating step was purposely kept short (45 min), in order to keep NRVFs residuals in the isolated stock NRVMs suspension. This is because a moderate presence of fibroblasts has been shown to support NRVMs networks in 3D, which facilitates CSs formation (Beauchamp et al., 2020).

By using three different ratios of cardiac cells, three distinct types of CSs were prepared as reported in Table 1. The stock NRVMs was used for the control, 7 parts of stock NRVMs, and 3 parts of stock NRVFs were mixed to generate the 70% NRVMs, while a 1:1 mixing ratio between the two stocks was used to create 50% NRVMs.

For the above-mentioned reasons, these percentages do not precisely represent the real amount of NRVMs inside the spheroid, but the mere number of cells coming from the NRVMs stock solution with respect to the total number of cells used to create the spheroid. In particular, in the case of CSs with 100% NMRVs, fibroblasts residuals are also present.

CSs were formed via the hanging drop method (Foty, 2011). For that,

Table 1
Nominal cell percentage to develop CSs. After four-days in 2D plates, NRVMs and NRCFs were harvested and CSs were created by using 50′000 NRVMs (100% cardiomyocytes, the control sample, namely CTRL), 35′000 NRVMs with 15′000 NRVFs (70% cardiomyocytes, intermediate fibrotic sample, namely F^+), and 25′000 NRVMs with 25′000 NRVFs (50% cardiomyocytes, advanced fibrotic sample, namely F^{++}).

Cell type	CTRL	F^+	F^{++}
Stock NRVM	100 %	70 %	50 %
Stock NRVF	–	30 %	50 %

20 μL drops of either 100%, 70%, or 50% high-density cell suspensions were pipetted on the inner side's lid of a 96 mm ø tissue culture dish, forming at least ten drops per sample, spaced 1 cm apart and containing approximately 50′000 cells each. Finally, the lid was rapidly flipped onto the dish's bottom, which had been previously filled with sterile PBS, thus leaving the drops hanging in a humidified environment. The cells in each drop assembled over the course of 4 days at 37 °C, 5% CO_2, forming co-cultured NRVMs/NRVFs cardiac spheroids.

2.4. Immunofluorescence (IF)

A multichannel immunostaining was used to visualize the composition of CSs. Fibroblasts were labeled by targeting Vimentin (Vim) (Humeres et al., 2019), while cardiomyocytes by Sarcomeric α-Actinin (α-Act). First, the CSs were fixed in PFA 4% for 1 h and permeabilized for 1 h 30 min (Triton X-100, 1%) at RT. Epitopes were blocked using 1% Bovine Serum Albumin (BSA) for 1 h at 4 °C. Primary antibody incubation was done overnight at 4 °C using a mixture of mouse anti Sarcomeric α-Actinin and chicken anti Vimentin mAbs (Abcam® ab9465 and ab24525 respectively, 1:200 dilution) in blocking buffer. Secondary fluorescent antibodies (Alexa Fluor 488 anti-mouse, Cy5 anti-rabbit, Abcam® ab150113 and ab6564 respectively, 1:1000 dilution) were then incubated for 1 h 30 min at RT. To counterstain the nuclei 5 μM DAPI (Sigma® D9542) was used, and the spheroids were imaged using Structured Illumination Microscopy (SIM).

For SIM, an Axio Observer Z1 inverted microscope with an ApoTome® module (1.6/1.5 transmission grid) and an AxioCam 506 monochrome camera were used (Carl Zeiss AG) to optically section spheroids through a 63x/1.4 EC Plan Neofluar oil immersion objective. Seven grid projection images were taken in 9–12 tiles at the lower, middle, and upper Z-slices of the spheroid. The images were then reconstructed using ZEN black edition by performing ApoTome® deconvolution and tile fusion.

2.5. NRVFs/NRVMs ratio quantification from IF

Starting from the optical sections, Vimentin (Vim, magenta) and Sarcomeric α-Actinin (α-Act, green) channels were isolated and separately thresholded using Fiji v2.9.0 (Rasband). Then, three squared regions of interest (ROI) of 100′000 μm^2 each were randomly placed on three areas of the spheroids' outer boundary, accounting for a potentially uneven fluorophore penetration rate. The Vim-stained area was finally referenced to the aggregated stained area (i.e., the sum of Vim and α-Act-stained areas).

2.6. Estimation of CSs size

The optical images acquired prior to each stress-relaxation experiment were processed with Fiji (example in Fig. 4a). For each spheroid, a circular ROI was manually drawn over its outer boundary. For slightly-elliptically shaped spheroids, an elliptical ROI was used. Then, each ROI's area was measured, and the diameter computed as:

$$d = 2 \bullet \sqrt{\frac{A}{\pi}}$$

Therefore, the elliptical spheroids were treated as they were spherical for the diameter estimation.

2.7. Whole-spheroid stress-relaxation by AFM

To measure CSs viscoelasticity, a NanoWizard II AFM equipped with a CellHesion module (JPK Instruments AG) was used. On the fourth day of culture, spheroids diameters were ranging between 200 and 400 μm. A single CS was retrieved and placed in the center of a 35 mm ø tissue culture dish filled with complete media and supplemented with 25 mM Hepes. The spheroid was approached to the macro probe establishing a weak contact with 5 nN force. Then, the Z-piezo was suddenly (500 ms) extended by 30 μm, and immediately locked in position. The vertical deflection (i.e., the force measured by the AFM) was monitored over 30 s to quantify the relaxation pattern of the squeezed CS. Then, the piezo was fully retracted and, after 5s of recovery, the spheroid was loaded again for at least 9 additional stress-relaxation cycles. At least 4 CSs per sample group (i.e., four CTRL, four F^{+}, and four F^{++}) were probed over three independent experimental replicates.

2.8. Viscoelasticity quantification

Following the sudden deformation and strain maintenance over time, we analyzed the resulting stress decay by using the generalized Maxwell model. A single Maxwell element is made up by a spring and dashpot placed in series. Therefore, an application of a load induces an immediate deflection by the elastic spring which is followed by a viscous time-dependent retardation by the dashpot. On the contrary, when a deformation is imposed, it produces an immediate reaction of the spring succeeded by stress relaxation following an exponential law (Fung, 2013). Therefore, a Maxwell material is a typical example of a material displaying viscoelastic properties, thus owning both elastic and viscous contributes. However, as observed in our previous studies (Zanetti et al., 2022; Andolfi et al., 2019; Battistella et al., 2022), the relaxation of CSs is characterized by a bi-exponential force decay. Therefore, the stress-relaxation curves were analyzed by a model combining 2 Maxwell elements and a single spring in parallel, hence via its generalized form. Such model assumes that, as the CSs are subjected to a constant deformation, the contact area does not change during the measurement, and the force decays following the equation:

$$F(t) = a_0 + a_1 \bullet e^{-\frac{t-t_0}{\tau_1}} + a_2 \bullet e^{-\frac{t-t_0}{\tau_2}}$$

where $\boldsymbol{\tau} = \eta/E$ ($\boldsymbol{\tau}$ is the relaxation time, η is the viscosity, and E is the Young's Modulus). To quantify such relaxation times ($\boldsymbol{\tau}_1$ and $\boldsymbol{\tau}_2$), a least-square batch curve fitting procedure was performed using a custom procedure in Igor Pro 8.0 (Wavemetrics Inc.)

2.9. Statistical data analysis

Nonparametric Dunn's test was performed in order to assess statistical differences between samples regarding the spheroids diameter and relaxation times. Sperman's rank order correlation was performed to evaluate spheroids diameter – relaxation time correlation, as well as the correlation between the first and the second relaxation time for each sample. All tests were carried out with Graphpad Prism®.

2.10. Second Harmonic Generation (SHG)

SHG imaging was carried out on fixed samples using a confocal Nikon® A1 MP + equipped with a 25x Apo water-immersion objective (NA 1.1) and a Chameleon Vision II (Coherent®) tunable laser (680–1080 nm, 3 V max.) set at 880 nm for collagen visualization.

To highlight the spheroids boundaries, images segmentation was performed by using the segmentation plugin implemented in Fiji. At the same time, the surface collagen distribution was qualitatively analyzed by using the surface plot tool of Fiji.

3. Results

In this work, 3D spheroids were employed as *in-vitro* models to investigate the viscoelastic hallmarks of MF. For such purpose, cardiomyocytes and fibroblasts were mixed at three different ratios, mimicking three distinct phenomena: a *physiological* tissue (CTRL), an intermediate MF (F^{+}), and an advanced MF (F^{++}). A schematic representation of CSs preparation is shown in Fig. 1.

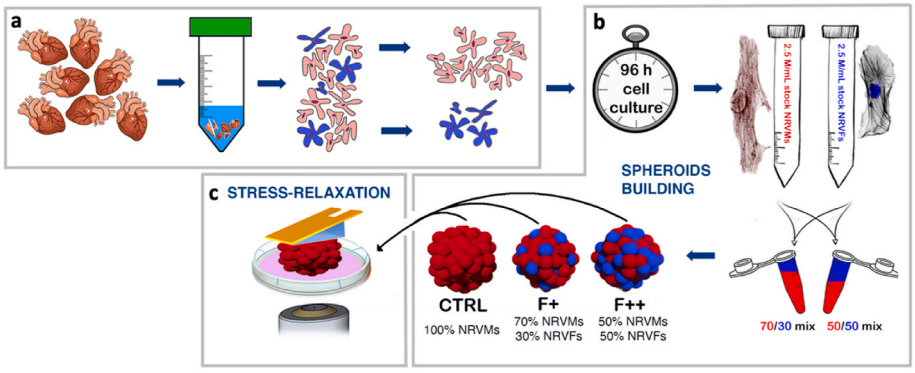

Fig. 1. Experimental workflow from cells isolation to AFM stress-relaxation experiment. The tissue digestion and NRVMs/NRVFs isolation steps (a). The 4-days 2D cell culture of both cell phenotypes (summarized as a pocket watch), NRVMs/NRVFs mixing at different ratios, and co-culture spheroids assembly (b). Schematic representation of the resulting CSs measured by AFM stress-relaxation (c).

After 4 days of hanging drop culture, spheroids were fully formed. As specified in Material and Methods, the nominal percentage of NRVMs (100% for CTRL, 70% for F^{+}, and 50% for F^{++}) did not represent the real ratio of cardiomyocytes into the spheroid but a mere approximation of it. At this stage, it was unclear whether cardiac fibroblasts could proliferate within the spheroid, and if so, what the proliferation rate would have been. Therefore, our first goal was to verify the cellular distribution.

3.1. *Mechanically activated fibroblasts proliferate in 3D*

To investigate the cell distribution within the spheroids, an optical sectioning was performed using SIM. NRVMs were labeled for Sarcomeric α-Actinin (α-Act), while NRVFs were labeled for Vimentin (Vim), which is a specific well-known fibroblasts marker not expressed in cardiomyocytes (Humeres et al., 2019; Tsikitis et al., 2018). Sections of the stained samples are shown in the images of Fig. 2a.

The presence of vimentin-stained filaments inside the CTRL spheroid confirms the occurrence of fibroblasts even in the 100% NRVMs spheroids which supports what already introduced previously regarding NRVFs residues. On the other hand, a progressive increase of NRVFs density into fibrotic spheroids was observed, as expected. The exact number of fibroblasts cannot be drawn just from estimating the Vim-stained area, but we can reasonably assume that the number of NRVMs does not change significantly after seeding, due to their limited proliferative capabilities. Therefore, if the NRVMs population is constant, we can use proportions to assess the proliferative behavior of NRVFs population. By comparing the Vim-stained area with the total amount of staining (Vim + α-Act), we observe that the ratio between fibroblast intermediate filaments and cardiomyocytes' sarcomeric proteins notably increases above 60% for both fibrotic spheroids (Fig. 2b). This evidence may seem trivial at first, because fibrotic spheroids were obtained by deliberately mixing a higher number of NRVFs with respect to NRVMs in the first place. However, if the higher number of seeded NRVFs was the sole reason for the relative greater Vim expression, it would be hard to explain the reason why F^{+} shows a comparable Vim staining ratio of F^{++} (61% vs 71% respectively), given that the latter was obtained using ~1.7x more fibroblasts (and ~1.4x less cardiomyocytes) than F^{+}. Therefore, especially for F^{+}, NRVFs must be proliferating inside the spheroid and actively producing more Vim. In addition, it is likely that NRVMs die into fibrotic spheroids, leaving unoccupied space for the fibroblasts to proliferate. This kind of NRVMs necrosis represents a well-

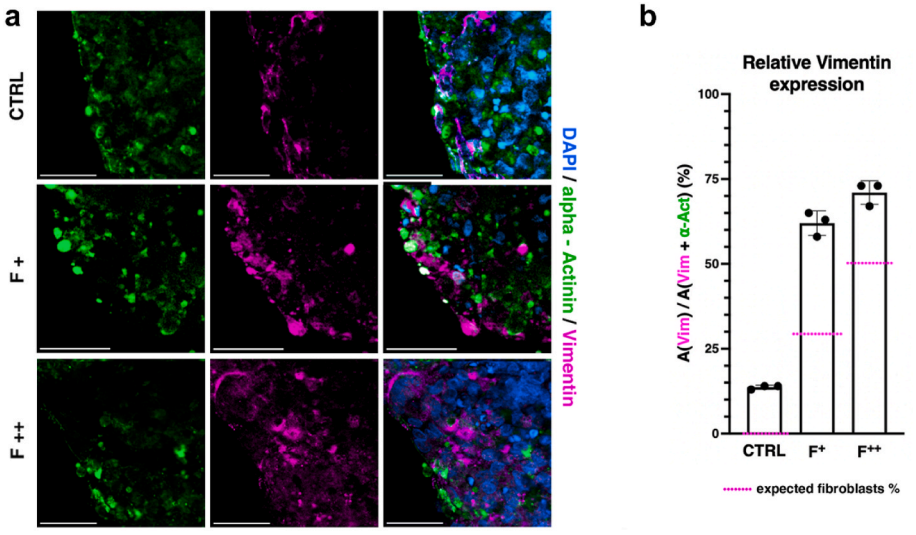

Fig. 2. SIM images of CSs and signal quantification. (a) Shows representative IF optical sections obtained by SIM in the case of physiological-like (CTRL), moderate fibrotic (F +) and advanced fibrotic (F ++) spheroids. DAPI-stained nuclei are shown in blue, ***α***-Actinin positive cells (cardiomyocytes) are shown in green, Vimentin positive cells (fibroblasts) are shown in magenta. Scale bar: 100 μm. (b) Shows the relative stained area of Vimentin normalized by the total stained area (Vimentin + ***α***-Actinin). Magenta dashed lines are the theoretical fibroblast amount, expressed as the theoretical percentage of fibroblasts as assembled into the spheroid (0, 30, and 50% for CTRL, F +, and F ++, respectively). Dots represent 100 × 100 μm averaged area counts, as taken from three distinct spheroids per each group. Bars show the Mean and whiskers SD.

known process of the heart fibrotic remodeling (Piek et al., 2016; Kong et al., 2014). Necrosis may also be induced by core hypoxia, although it is unlikely to occur in our conditions due to the relatively small size our spheroids. Indeed, hypoxic conditions were noticed in tumor spheroids larger than 500–600 μm (Kim et al., 2021; Riffle et al., 2017). Similarly, in cardiac spheroids, a hypoxic core was observed in spheroids with a diameter of at least 500 μm (Paz-Artigas et al., 2024). Finally, due to the initial lower presence of NRVMs into F^{++} spheroids with respect to F^{+}, the NRVFs proliferation might result favoured in F^{+} CSs, where more available space would arise as consequence of NRVMs death.

Indeed, recent ex-vivo cases of ischemic heart disease showed elevated Vim expression around myocardial cells undergoing remodeling (Kondo et al., 2022). At the same time, a growing amount of research pinpoints how the mechanical interaction between cells and culture surface plays a crucial role in shaping the phenotypical transition of different cell types, by changing their mechanical and morphological properties (Nasrollahi et al., 2017; Zhuang et al., 2022; Yeh et al., 2017). For example, primary rat cardiac fibroblasts have shown to incorporate pro-fibrotic α-SMA into their stress fibers when cultured onto >10 kPa substrates, representative of phenotypic conversion into myofibroblasts (Landry et al., 2019; Ceccato et al., 2020; Zhao et al., 2014). Moreover, cell proliferation has been demonstrated to be controlled by mechanical extracellular features as shown in (Landry et al., 2019; Zhao et al., 2014; Ebrahimighaei et al., 2022). Therefore, a softer culture substrate would be needed to maintain fibroblasts physiological features, preventing their pro-fibrotic activation.

In our work, we leveraged this otherwise detrimental mechanical interaction by pre-expanding the NRVFs population on a 2D stiff plastic surface, thus mechanically pre-activating the fibroblasts before the 3D NRVMs co-culture. Our experimental results demonstrate a proliferative stage inside F^{+} CSs, suggesting that our multi-step 2D/3D approach represents a suitable workflow to induce the proliferative stage of MF *in vitro*.

3.2. Spheroid rheology is altered in MF models

Traditional approaches to assess cellular mechanics have predominantly focused on measuring cell elasticity, overlooking the dynamic nature of cellular responses to mechanical stimuli. However, cells exhibit a complex viscoelastic behavior, characterized by both elastic (deformation) and viscous (flow) components (Gerum et al., 2022). This dynamic behavior arises from the intricate interplay of cellular components, including cytoskeletal proteins, intercellular adhesions, and ECM interactions. Therefore, measuring the viscoelastic properties of cells, and their dimensional spaced-aggregates (as for 3D cellular spheroids), provides a more comprehensive understanding of their mechanical behavior compared to traditional elasticity measurements alone.

To characterize CSs viscoelasticity, we performed stress-relaxation uniaxial loadings by means of AFM while modeling the spheroid as a Maxwell material. If we assume a single Maxwell element is subjected to a sudden deformation, and maintained at a constant strain, then the stress will experience a decay on a timescale of $\tau = \eta/E$. However, a single Maxwell element was not sufficient to fully reproduce the relaxation pattern of neither CTRL nor F^{+} and F^{++} CSs, leading to poor data fitting. Instead, we observed that the stress-relaxation curves follow a two-phase decay. Therefore, they were fitted to a two-component generalized Maxwell model with two distinct relaxation times. The outcoming response was characterized by a quick relaxation that lasted up to a second, followed by a slower viscous dissipation (Fig. 3a). Such behavior has been also previously observed in our studies on hanging-drop cultured cardiomyocytes (Zanetti et al., 2022), tumor spheroids (Andolfi et al., 2019), oocytes (Battistella et al., 2022) and keratinocytes (Puzzi et al., 2018), and also by other authors (Moreno-Flores et al., 2010a, 2010b; Maares et al., 2020; Zbiral et al., 2023).

Generally, both relaxation times show a lowering trend in the case of fibrotic spheroids (F^{+} and F^{++}), when compared to control (Fig. 3b and c). The first relaxation time τ_1 is statistically shorter for F^{++} spheroids compared to control (Fig. 3b), while τ_2 shows the same trend without being statistically significant (Fig. 3c). To better highlight the magnitude of times reduction, especially for the first one, τ_1 was referenced to the total relaxation time (i.e., $\tau_1 + \tau_2$) as shown in Fig. 3d. The relative effect is even more pronounced, with a fast relaxation time accounting for 7.88 ± 0.55% of the total measured relaxation time for F^{++}, and a greater percentage of 9.04 ± 0.9% in the case of the control.

These results point out that τ_1 may represent an important parameter in the discrimination between physiological and fibrotic spheroids, further confirming a rheological imbalance between the two. However, the viscoelastic behavior of the CS could also be influenced by a variation in the spheroid diameter, hence the need to rule out the "size" confounding factor.

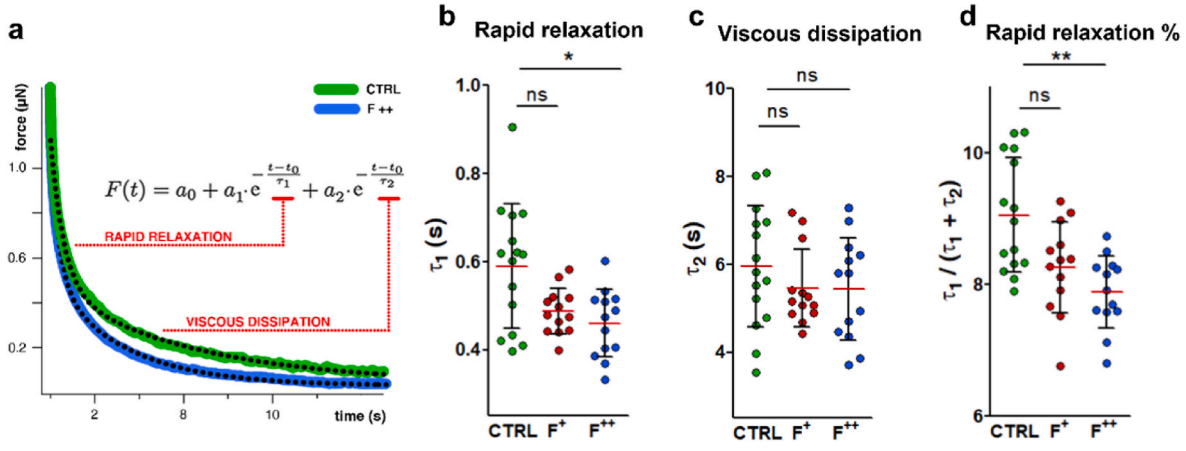

Fig. 3. Biexponential behavior of CSs as revealed by AFM stress-relaxation measurements. Exemplificative AFM relaxation curves of a CTRL (green) and advanced fibrotic F^{++} (blue) spheroids (a). Only the first 15 s are shown, to further highlight the trend variation. Dashed lines are the fitting curves as obtained through least-square fitting of the two-component Generalized Maxwell model, used to extrapolate the rapid relaxation time (τ_1), and the longer one (τ_2). Each spheroid's first relaxation time per each condition, CTRL vs F^{++} times are statistically different ($p = 0.0157$) (b), the same as, but for the second relaxation time (c). The ratio of the first (τ_1) divided by the sum ($\tau_1 + \tau_2$) of both relaxations. CTRL vs F^{++} ratios are statistically different ($p = 0.0012$) (c). All the statistics were carried out by Dunn's nonparametric pairwise comparison. Dots represent a single measured spheroid (green for CTRL, red for F^{+}, and blue for F^{++}). Red lines at Mean, black whiskers are SDs.

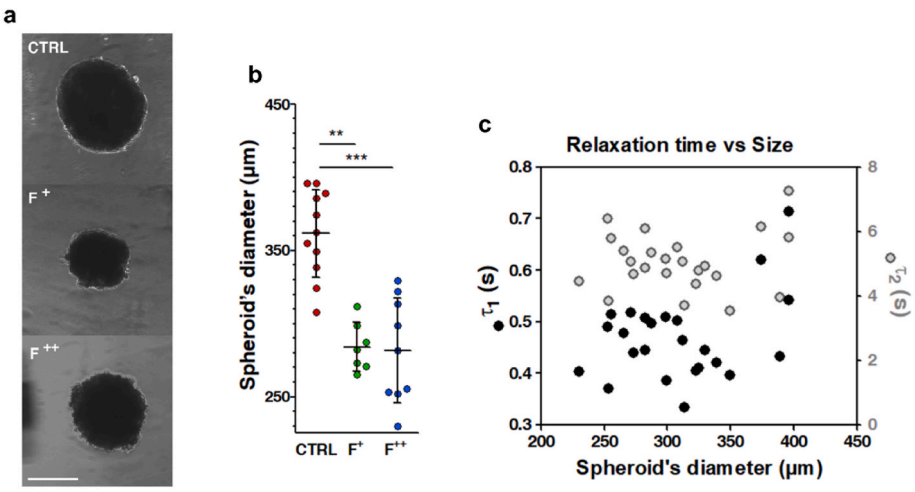

Fig. 4. CSs diameters and relaxation time dependence on these. Three representatives bright field images of the spheroids (a), and the diameter distribution of the CTRL, F+, and F++ populations, (b) which are statistically different as shown by pairwise nonparametric Dunn's test ($p = 0.0019$ for CTRL vs F+, and $p = 0.0007$ for CTRL vs F++). Bars represent Mean, whiskers represent SD. Scale bar: 100 µm. The first and second relaxation times (each dot represents a spheroid) plotted against the spheroid diameter (c). No correlation of either first or second relaxation times with the spheroid diameter was observed through Spearman's rank order correlation statistics. Spearman's r (22) = 0.11, p = 0.60, 95% CI [-0.32, 0.50] and Spearman's r (22) = −0.027, p = 00.90, 95% CI [-0.44, 0.39] for $\tau 1$ and $\tau 2$ respectively.

3.3. Size does not affect the measured viscoelasticity of CSs

To test whether the stress-relaxation behavior could be affected by the size of the CSs we analyzed the correlation between size and the relaxation times (τ_1 and τ_2). In principle, the inner composition can influence the spheroid's size, because NRVMs and NRVFs differ in cellular volume with the first resulting larger than second ones (Zhou et al., 2016) while occupying a confined 3D space. In fact, a reduced number of NRVMs in our fibrotic spheroids led to a reasonable volumetric shrinkage for both, as assessed by optical microscopy (Fig. 4a).

If we focus on the cell number alone, and assuming that the NRVMs number keeps constant from cell seeding, while activated NRVFs proliferate at similar rates among the groups, we would expect a progressive decrease in volume, with the control group being the largest, followed by F^+, and then F^{++}. However, while the spheroid's diameter is significative greater for the control group (362 ± 30) µm compared to (284 ± 17) µm for F+ and (282 ± 36) µm for F^{++}, the fibrotic CSs show no significant size differences between each other (Fig. 4b). In agreement with what we previously anticipated, this could be likely due to the loss of NRVMs, which leave unoccupied space available for fibroblasts proliferation, which preferentially occurs in F^+ respect to F^{++} spheroids. However, since cardiac fibroblasts occupy a smaller volume with respect to NRVMs, the space previously occupied by NRVMs would never be totally replaced, thus inducing the CSs shrinkage. Moreover, due to the limited presence of NRVMs in the F^{++} cardiac spheroids, this phenomenon is less pronounced and therefore this results in an almost equal volume of F^+ and F^{++}, matching the previous results about fibroblasts proliferation by monitoring Vim signal.

As previously mentioned, the size variability among the spheroids can have a significant impact on their viscoelastic properties. In fact, the initial applied stress is not only influenced by the composition of the biological material and the constant Z-piezo displacement, but also by the volume of the spheroid itself. Indeed, if we keep the same Z-displacement, a larger spheroid would eventually be less stressed than a smaller one. In order to assess this factor, a correlation analysis was performed, to examine the relationship between the relaxation times (τ_1 and τ_2 as calculated from the fitting procedure) and the diameter of the spheroids across all groups (as depicted in Fig. 4c).

While the diameters distribution for F^+ and F^{++} respect to CTRL is significantly different, both τ_1 and τ_2 showed to be neither positively nor negatively correlated with the spheroid's diameter among all CSs types. The absence of correlation between the measured viscoelastic decays and the spheroid's diameter further confirms that our AFM-based approach investigates the CS viscoelasticity without being remarkably affected by its size, at least in the 200–400 µm range, consistently with what we previously observed with tumor spheroids (Andolfi et al., 2019).

3.4. The ECM deposition affects viscoelasticity in the CSs

Since it is widely known that ECM accumulation in MF causes stiffening of the heart muscle (Aghajanian et al., 2019; Travers et al., 2016; López et al., 2021), we investigated whether the relaxation times might be influenced by enhanced ECM deposition caused by fibroblasts. For this purpose, we performed Second Harmonic Generation (SHG) for collagen distribution assessment and found an increased collagen signal for F^{++} spheroid with respect to F^+ (Fig. 5). In fact, F^+ spheroids display spotted regions in the image indicating a discretized collagen signal (Fig. 5a), while for F^{++} we observed a continuous and diffuse signal which is an indication of massive collagen layer which envelops the whole spheroid (Fig. 5b). In support of this we also performed a surface image analysis which confirmed the discrete nature of the signal coming from F^+ spheroid with respect to the broad and smoothed one coming from F^{++} (see Supplementary Fig. S1). This might result as a progressive accumulation process starting soon after the CSs assembly due to the higher NRVFs content.

Therefore, we can conclude that the higher collagen deposition in F^{++} CSs induces ECM-driven CSs stiffening which in turn can strongly influence the CSs rheology by modulating the relaxation times.

4. Discussion

In this work we shaped the myocardium into a multicellular 3D spheroid and investigated its viscoelastic behavior through AFM stress-relaxation experiments. To our knowledge, this is the first time in which the fibrotic pathophysiological features are naturally recapitulated without making any use of profibrotic treatments. Firstly, we found that pre-culturing cells on 2D hard surfaces promote fibrotic proliferation in 3D, which is a key feature of myocardial fibrosis (Liu et al., 2023). In particular, we specifically observed activated myofibroblasts increased proliferation in intermediately fibrotic loci (F^+). We found this feature compatible with the increased unoccupied space left free by necrotic

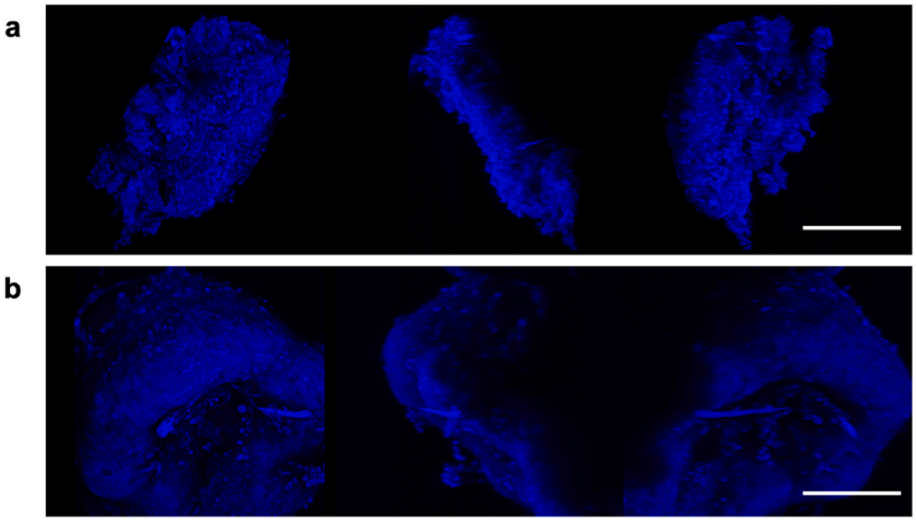

Fig. 5. Collagen distribution for F+ and F++ spheroids. Second Harmonic Generation images of F+ (a) and F++ (b) spheroids. CSs rotation along z direction with frames corresponding to steps of 120° for a total 360° rotation. Scale bar: 200 μm.

cardiomyocytes (Piek et al., 2016; Kong et al., 2014). Moreover, in diffuse fibrotic loci (F^{++}), myofibroblasts actively increased the collagen production, as demonstrated by SHG, which is likely correlated to CSs stiffening. In fact, collagen deposition is well-known to contribute to myocardial stiffening (Jalil et al., 1989; Cowling et al., 2019) and can promote rheological impairment. We, therefore, can attribute this increased collagen production to the observed differences in the relaxation times. In single cells, the two relaxation times have been associated to different components dynamic, with the first one referring to the dynamic of "individual units" (e.g. the cell membrane) and the second one to the collective dynamic of the whole (e.g. cytoskeletal rearrangement) (Moreno-Flores et al., 2010a, 2010b; Maares et al., 2020). Thus, the increased collagen deposition observed at the outer side of F^{++} spheroids can elevate the elastic modulus (E) and resulting in turn in a lower τ. In fact, for both fibrotic (F^{+} and F^{++}) spheroids we observed a reduction in relaxation times, although a strong significant reduction was only observed for τ_1 in F^{++} with respect to CTRL. Therefore, our model can precisely simulate the natural ECM deposition in fibrotic condition which influences the overall rheological properties.

On the other hand, the second relaxation time (τ_2) accounts for the whole system dynamic during which cells are supposed to reorganize themselves to adapt to the newly confined space. To do so, they are required to break and reform their adhesive contacts like the ones sustained by integrins and cadherins (Matsushita et al., 1999). Looser adhesive contacts will reflect to a lower adhesion energy and, therefore, to a faster relaxation time. Even though we did not address specifically the adhesive molecules in our experiment, integrins and cadherins are known for being more expressed in fibrotic tissue (Riley et al., 2021; Meagher et al., 2021). Therefore, the trend we found for τ_2 seems paradoxical, as we would have expected longer dissipation times for fibrotic spheroids, given the hypothetical greater adhesion between cells. Nevertheless, it must be considered that τ_2 distributions are more dispersed throughout all groups. Moreover, while τ_1 have been associated mainly to the ECM response, and τ_2 to the cellular adhesive remodeling, we should avoid oversimplifying these two parameters by minimizing them to a discrete overview since they depend on both elastic and viscous characters, which we are unable to decouple.

In conclusion, our study highlights the importance of developing improved models and techniques to better understand the underlying mechanisms of myocardial fibrosis. MF is a serious pathological condition in need of new specific therapies, pushing the efforts towards the acquisition of deeper knowledge on fibrotic mechanisms, especially the characterization of the mechanical implicated features. Therefore, we believe that the combination between a 3D co-culture model and our proposed AFM macro-cantilevers represents a step forward in this field and may be useful in developing new strategies for the treatment of this globally detrimental disease.

CRediT authorship contribution statement

Michele Zanetti: Writing – review & editing, Writing – original draft, Visualization, Project administration, Methodology, Investigation, Formal analysis, Data curation, Conceptualization. **Nicoletta Braidotti:** Writing – review & editing, Writing – original draft, Visualization, Methodology, Investigation, Formal analysis, Data curation, Conceptualization. **Maydha Khumar:** Methodology, Investigation. **Efren Montelongo:** Methodology, Investigation. **Raffaella Lombardi:** Validation. **Orfeo Sbaizero:** Supervision. **Luisa Mestroni:** Writing – review & editing, Supervision, Resources, Funding acquisition, Conceptualization. **Matthew R.G. Taylor:** Supervision, Resources, Funding acquisition. **Gabriele Baj:** Writing – review & editing, Methodology, Investigation. **Marco Lazzarino:** Validation, Supervision, Resources, Funding acquisition, Conceptualization. **Brisa Peña:** Writing – review & editing, Supervision, Resources, Funding acquisition. **Laura Andolfi:** Writing – review & editing, Validation, Supervision, Resources, Project administration, Funding acquisition.

Declaration of competing interest

The authors declare that they have no known competing financial interests or personal relationships that could have appeared to influence the work reported in this paper.

Data availability

Data will be made available on request.

Acknowledgements

We acknowledge the Italian Liver Foundation (Fondazione Italiana Fegato ONLUS, Trieste), for the donation of the excess animal tissues, allowing us to work in a sustainable way. In particular, we thank Silvia Gazzin, Sri Yayanti, and Claudio Tiribelli.

This study was supported by the PRIN2020 - Toac project (B53C22001570006) MUR-Italy.

For the international mobility, M.Z. acknowledges Nano-Region, an

Interreg V-A Italy-Slovenia 2014–2020 strategic project supported by the Italy-Slovenia Cooperation Programme of the European Regional Development Fund of the EU. This research was also funded by the National Institutes of Health (NIH) National Heart, Lung, and Blood Institute (NHLBI): grants K25HL148386 (B.P.), R01HL169578 (B.P.) and R01HL147064 and R01HL164634 (L.M.), the NIH National Institute of Aging (NIA) R21AG080257 (B.P.), the Ludeman Family Center for Women's Health Research seed grant (B.P.), the American Heart Association (AHA): 23CDA1052411 (B.P.). This study was also supported by generous grants of the John Patrick Albright (L.M., M.T. and B.P.)

M.Z. and N.B. acknowledge the University of Trieste and the Material's Foundry Institute CNR-IOM for the provided co-funding in the framework of the Nanotechnology PhD program.

Finally, we thank Marcello Rubino for the useful and stimulating discussions about fibroblasts and their remodeling features.

Appendix A. Supplementary data

Supplementary data to this article can be found online at https://doi.org/10.1016/j.jmbbm.2024.106571.

References

Aghajanian, H., et al., 2019. Targeting cardiac fibrosis with engineered T cells. Nature 573 (7774), 430–433.
Andolfi, L., et al., 2019. Planar AFM macro-probes to study the biomechanical properties of large cells and 3D cell spheroids. Acta Biomater. 94, 505–513.
Andolfi, L., et al., 2023. X-rays induced alterations in mechanical and biochemical properties of isolated SH-SY5Y nuclei. Biochim. Biophys. Acta Gen. Subj. 1867 (3), 130291.
Battistella, A., et al., 2022. Atomic force spectroscopy-based essay to evaluate oocyte postovulatory aging. Bioengineering & translational medicine 7 (3), e10294.
Beauchamp, P., et al., 2020. 3D Co-culture of hiPSC-derived cardiomyocytes with cardiac fibroblasts improves tissue-like features of cardiac spheroids. Front. Mol. Biosci. 7, 14, 14.
Braidotti, N., et al., 2022. The role of cytoskeleton revealed by quartz crystal microbalance and digital holographic microscopy. Int. J. Mol. Sci. 23 (8), 4108.
Ceccato, T.L., et al., 2020. Defining the cardiac fibroblast secretome in a fibrotic microenvironment. J. Am. Heart Assoc. 9 (19), e017025.
Cheng, S., Clarke, E.C., Bilston, L.E., 2008. Rheological properties of the tissues of the central nervous system: a review. Med. Eng. Phys. 30 (10), 1318–1337.
Chim, Y.H., et al., 2018. A one-step procedure to probe the viscoelastic properties of cells by Atomic Force Microscopy. Sci. Rep. 8 (1), 14462.
Cowling, R.T., et al., 2019. Mechanisms of cardiac collagen deposition in experimental models and human disease. Transl. Res. : J. Lab. Clin. Med. 209, 138–155.
Davidson, M.D., Burdick, J.A., Wells, R.G., 2020. Engineered biomaterial platforms to study fibrosis. Adv. Healthcare Mater. 9 (8), e1901682.
Demer, L.L., Yin, F.C., 1983. Passive biaxial mechanical properties of isolated canine myocardium. J. Physiol. 339 (1), 615–630.
Diamond, J.A., Phillips, R.A., 2005. Hypertensive heart disease. Hypertens. Res. 28 (3), 191–202.
Ebrahimighaei, R., et al., 2022. Combined role for YAP-TEAD and YAP-RUNX2 signalling in substrate-stiffness regulation of cardiac fibroblast proliferation. Biochim. Biophys. Acta Mol. Cell Res. 1869 (11), 119329.
Emig, R., et al., 2021. Passive myocardial mechanical properties: meaning, measurement, models. Biophysical reviews 13 (5), 587–610.
Figtree, G.A., et al., 2017. Vascularized cardiac spheroids as novel 3D in vitro models to study cardiac fibrosis. Cells Tissues Organs 204 (3–4), 191–198.
Foty, R., 2011. A simple hanging drop cell culture protocol for generation of 3D spheroids. J. Vis. Exp. (51), 2720.
Frangogiannis, N.G., 2021. Cardiac fibrosis. Cardiovasc. Res. 117 (6), 1450–1488.
Fung, Y.C., 2013. Biomechanics: Mechanical Properties of Living Tissues. Springer, New York.
Gerum, R., et al., 2022. Viscoelastic properties of suspended cells measured with shear flow deformation cytometry. Elife 11, e78823.
Gheorghiade, M., et al., 2006. Navigating the crossroads of coronary artery disease and heart failure. Circulation 114 (11), 1202–1213.
Guo, Y., et al., 2021. The Ca(2+)-activated cation channel TRPM4 is a positive regulator of pressure overload-induced cardiac hypertrophy. Elife 10, e66582.
Hassan, M.A., Hamdi, M., Noma, A., 2012. The nonlinear elastic and viscoelastic passive properties of left ventricular papillary muscle of a Guinea pig heart. J. Mech. Behav. Biomed. Mater. 5 (1), 99–109.
Humeres, C., Frangogiannis Nikolaos, G., 2019. Fibroblasts in the infarcted, remodeling, and failing heart. JACC (J. Am. Coll. Cardiol.): Basic to Translational Science 4 (3), 449–467.
Jalil, J.E., et al., 1989. Fibrillar collagen and myocardial stiffness in the intact hypertrophied rat left ventricle. Circ. Res. 64 (6), 1041–1050.
Kim, B.S., et al., 2021. Construction of tissue-level cancer-vascular model with high-precision position control via in situ 3D cell printing. Small Methods 5 (7), 2100072.
Kondo, T., et al., 2022. Immunohistochemical analysis of vimentin expression in myocardial tissue from autopsy cases of ischemic heart disease. Leg. Med. 54, 102003.
Kong, P., Christia, P., Frangogiannis, N.G., 2014. The pathogenesis of cardiac fibrosis. Cell. Mol. Life Sci. : CM 71 (4), 549–574.
Landry, N.M., Rattan, S.G., Dixon, I.M.C., 2019. An improved method of maintaining primary murine cardiac fibroblasts in two-dimensional cell culture. Sci. Rep. 9 (1), 12889.
Leask, A., 2007. TGFβ, cardiac fibroblasts, and the fibrotic response. Cardiovasc. Res. 74 (2), 207–212.
Liu, W., et al., 2022. Strain-dependent stress relaxation behavior of healthy right ventricular free wall. Acta Biomater. 152, 290–299.
Liu, X., et al., 2023. p53 regulates the extent of fibroblast proliferation and fibrosis in left ventricle pressure overload. Circ. Res. 133 (3), 271–287.
López, B., et al., 2021. Diffuse myocardial fibrosis: mechanisms, diagnosis and therapeutic approaches. Nat. Rev. Cardiol. 18 (7), 479–498.
Maares, M., et al., 2020. Time- and zinc-related changes in biomechanical properties of human colorectal cancer cells examined by atomic force microscopy. Biology 9 (12), 468.
Mahaffy, R.E., et al., 2004. Quantitative analysis of the viscoelastic properties of thin regions of fibroblasts using atomic force microscopy. Biophys. J. 86 (3), 1777–1793.
Matsushita, T., et al., 1999. Remodeling of cell-cell and cell–extracellular matrix interactions at the border zone of rat myocardial infarcts. Circ. Res. 85 (11), 1046–1055.
Meagher, P.B., et al., 2021. Cardiac fibrosis: key role of integrins in cardiac homeostasis and remodeling. Cells 10 (4).
Moreno-Flores, S., et al., 2010a. Stress relaxation and creep on living cells with the atomic force microscope: a means to calculate elastic moduli and viscosities of cell components. Nanotechnology 21 (44), 445101.
Moreno-Flores, S., et al., 2010b. Stress relaxation microscopy: imaging local stress in cells. J. Biomech. 43 (2), 349–354.
Nasrollahi, S., et al., 2017. Past matrix stiffness primes epithelial cells and regulates their future collective migration through a mechanical memory. Biomaterials 146, 146–155.
Parkins, C.C., et al., 2021. Mechanically matching the rheological properties of brain tissue for drug-delivery in human glioblastoma models. Biomaterials 276, 120919.
Paz-Artigas, L., et al., 2024. Generation of self-induced myocardial ischemia in large-sized cardiac spheroids without alteration of environmental conditions recreates fibrotic remodeling and tissue stiffening revealed by constriction assays. ACS Biomater. Sci. Eng. 10 (2), 987–997.
Piek, A., de Boer, R.A., Silljé, H.H.W., 2016. The fibrosis-cell death axis in heart failure. Heart Fail. Rev. 21 (2), 199–211.
Polonchuk, L., et al., 2017. Cardiac spheroids as promising in vitro models to study the human heart microenvironment. Sci. Rep. 7 (1), 7005.
Puzzi, L., et al., 2018. Cellular biomechanics impairment in keratinocytes is associated with a C-terminal truncated desmoplakin: an atomic force microscopy investigation. Micron 106, 27–33.
Rasband, W.S. ImageJ. 1997-2018.; Available from: https://imagej.nih.gov/ij/..
Riffle, S., et al., 2017. Linking hypoxia, DNA damage and proliferation in multicellular tumor spheroids. BMC Cancer 17 (1), 338.
Riley, L.A., Merryman, W.D., 2021. Cadherin-11 and cardiac fibrosis: a common target for a common pathology. Cell. Signal. 78, 109876, 109876.
Rother, J., et al., 2014. Atomic force microscopy-based microrheology reveals significant differences in the viscoelastic response between malign and benign cell lines. Open Biology 4 (5), 140046.
Schultheiss, H.-P., et al., 2019. Dilated cardiomyopathy. Nat. Rev. Dis. Prim. 5 (1), 32.
Travers, J.G., et al., 2016. Cardiac fibrosis. Circ. Res. 118 (6), 1021–1040.
Tsikitis, M., et al., 2018. Intermediate filaments in cardiomyopathy. Biophysical Reviews 10 (4), 1007–1031.
Vukicevic, S., et al., 2022. Bone morphogenetic protein 1.3 inhibition decreases scar formation and supports cardiomyocyte survival after myocardial infarction. Nat. Commun. 13 (1), 81.
Yeh, Y.-C., et al., 2017. Mechanically dynamic PDMS substrates to investigate changing cell environments. Biomaterials 145, 23–32.
Zanetti, M., et al., 2022. AFM macro-probes to investigate whole 3D cardiac spheroids. Micro and Nano Engineering 15, 100134.
Zbiral, B., et al., 2023. Characterization of breast cancer aggressiveness by cell mechanics. Int. J. Mol. Sci. 24 https://doi.org/10.3390/ijms241512208.
Zhao, H., et al., 2014. Microengineered in vitro model of cardiac fibrosis through modulating myofibroblast mechanotransduction. Biofabrication 6 (4), 045009.
Zhou, P., Pu, W.T., 2016. Recounting cardiac cellular composition. Circ. Res. 118 (3), 368–370.
Zhuang, Y., et al., 2022. Effect of substrate stiffness on the mechanical properties of cervical cancer cells. Arch. Biochem. Biophys. 725, 109281.